A facile approach towards increasing the nitrogen-content in nitrogen-doped carbon nanotubes *via* halogenated catalystsg

L.M. Ombaka, P.G. Ndungu, B. Omondi, J.D. McGettrick, M.L. Davies, V.O. Nyamori

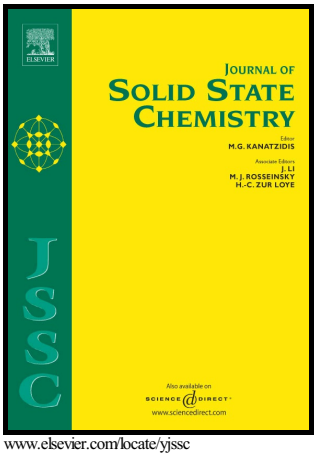

www.elsevier.com/locate/yjssc

PII: S0022-4596(16)30006-8
DOI: http://dx.doi.org/10.1016/j.jssc.2016.01.007
Reference: YJSSC19229

To appear in: *Journal of Solid State Chemistry*

Received date: 27 September 2015
Revised date: 15 December 2015
Accepted date: 11 January 2016

Cite this article as: L.M. Ombaka, P.G. Ndungu, B. Omondi, J.D. McGettrick M.L. Davies and V.O. Nyamori, A facile approach towards increasing the nitrogen-content in nitrogen-doped carbon nanotubes *via* halogenated catalystsg *Journal of Solid State Chemistry,* http://dx.doi.org/10.1016/j.jssc.2016.01.007

A facile approach towards increasing the nitrogen-content in nitrogen-doped carbon nanotubes *via* halogenated catalysts

L.M. Ombaka[1], P.G. Ndungu[1,2], B. Omondi[1], J.D. McGettrick[3], M.L. Davies[3], V.O. Nyamori[1*]

[1]School of Chemistry and Physics, University of KwaZulu-Natal, Westville Campus, Private Bag X54001, Durban, 4000, South Africa

[2]Department of Applied Chemistry, Doornfontein Campus, University of Johannesburg, P.O. Box 17011, Johannesburg, 2028, South Africa.

[3]SPECIFIC, Swansea University, Baglan Bay Innovation Centre, Baglan, Port Talbot, SA12 7AX, United Kingdom.

*****Corresponding author. Telephone: +27-31 260 8256; Fax: +27-31 260 3091

E-mail address: nyamori@ukzn.ac.za (V.O. Nyamori)

Abstract

Nitrogen-doped carbon nanotubes (N-CNTs) have been synthesized at 850 °C *via* a CVD deposition technique by use of three ferrocenyl derivative catalysts, i.e. *para*-CN, -CF_3 and -Cl substituted-phenyl rings. The synthesized catalysts have been characterized by NMR, IR, HR-MS and XRD. The XRD analysis of the *para*-CF_3 catalyst indicates that steric factors influence the X-ray structure of 1,1′-ferrocenylphenyldiacrylonitriles. Acetonitrile or pyridine was used as carbon and nitrogen sources to yield mixtures of N-CNTs and carbon spheres (CS). The N-CNTs obtained from the *para*-CF_3 catalysts, in pyridine, have the highest nitrogen-doping level, show a helical morphology and are less thermally stable compared with those synthesised by use of the *para*-CN and -Cl as catalyst. This suggests that fluorine heteroatoms enhance nitrogen-doping in N-CNTs and formation of helical-N-CNTs (H-N-CNTs). The *para*-CF_3 and *para*-Cl catalysts in acetonitrile yielded iron-filled N-CNTs, indicating that halogens promote encapsulation of iron into the cavity of N-CNT. The use of acetonitrile, as carbon and nitrogen source, with the *para*-CN and -Cl as catalysts also yielded a mixture of N-CNTs and carbon nanofibres (CNFs), with less abundance of CNFs in the products obtained using *para*-Cl catalysts. However, *para*-CF_3 catalyst in acetonitrile gave N-CNTs as the only shaped carbon nanomaterials.

Keywords: Helical nitrogen-doped carbon nanotubes; chlorine; fluorine; ferrocenyldiacrylonitriles; chemical vapour deposition.

1. Introduction

Shaped carbon nanomaterials (SCNMs) such as carbon nanotubes (CNTs) are fascinating carbonaceous materials with novel physical and chemical properties [1]. Owing to their unique properties, such as high tensile strength, Young's modulus [2], thermal stability [3], surface area [4], and excellent electrochemical properties [5], CNTs have been found to be useful materials in the field of nanotechnology [1]. These physicochemical properties of CNTs can be enhanced further *via* nitrogen-doping to form nitrogen-doped CNTs (N-CNTs) [6]. The nitrogen species present in N-CNTs act as n-type conductors and as basic functional groups thus enhancing the electrical properties [7] and surface energy [8] of N-CNTs. Additionally, N-CNTs contain defect sites that can improve their wettability and surface area [9] which are useful properties for potential application of N-CNTs in various fields such as catalysis [1] and field emission devices [10].

Unlike other flake-like carbonaceous materials such as graphene, CNTs and N-CNTs are cylindrical and contain hollow cavities in their structures. These hollow cavities can be filled with iron to form ferromagnetic CNTs and N-CNTs [11]. Ferromagnetic CNTs and N-CNTs are used in different areas, such as electromagnetic wave absorption [11]. They can also be applied as heterogeneous catalysts with the added advantage of the ease of separating them from solutions by use of magnets [12]. Iron filled CNTs have been synthesized by using mixtures of organic halogens and ferrocene as catalysts [13]. For instance, Gui *et al*. synthesized iron-encapsulated CNTs by use of dichlorobenzene and ferrocene catalyst [14]. However, little is known about the use of halogenated ferrocenyl derivatives as catalysts in the synthesis of iron encapsulated CNTs or N-CNTs.

Ferrocene [15] and ferrocenyl derivatives [16], due to their volatile nature, are frequently used as catalysts in the synthesis of CNTs and other shaped carbon nanomaterials (SCNMs) [15, 17]. Nitrogen-containing ferrocenyl derivatives, as catalysts, have been explored in the synthesis of N-CNTs [8]. In some instances, the use of nitrogen-containing ferrocenyl derivatives yields

N-CNTs with better physical or chemical properties as opposed to the use of ferrocene dissolved in a nitrogen containing organic solvent. For example, Nxumalo *et al*. showed that the use of 4-ferrocenylaniline as a catalyst yields N-CNTs with higher nitrogen-doping levels compared with ferrocene in aniline solution [18]. Another seldom-explored approach that can also be useful in modulating the nitrogen content and species in N-CNTs and other properties of SCNMs is the use of halogens [19]. Halogens, such as fluorine, are potential oxidizing agents that could induce defects in CNTs during the nucleation; these defect sites can easily accept nitrogen species resulting in higher nitrogen-doping levels. However, reports on the use of halogens to modulate nitrogen-content in N-CNTs are limited.

In this study, 1,1′-ferrocenyldiacrylonitriles (Fig. 1), containing nitrogen-(*para*-CN), fluorine- (*para*-CF_3) and chlorine-heteroatoms (*para*-Cl), were synthesized and characterized. The X-ray crystallographic structure of the *para*-CF_3 catalyst is reported for the first time. The 1,1′-ferrocenyl-diacrylonitriles have been investigated as novel catalyst for the synthesis of N-CNTs, carbon nanofibres (CNFs) and carbon spheres (CS). The chlorine and fluorine heteroatoms were used to evaluate the effect of halogenated catalysts on nitrogen-doping and iron encapsulation into the cavity of N-CNTs. We also present the effect of halogen heteroatoms on the diameters, type of nitrogen-species in N-CNTs and also the not only on amount of product but also the distribution of the products. The effect of varying the carbon and nitrogen source has been evaluated by using either acetonitrile or pyridine as the carbon and nitrogen source.

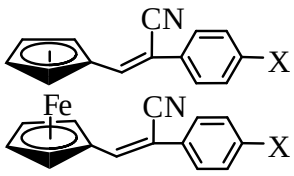

X=CN [*para*-CN catalyst]
X=CF_3 [*para*-CF_3 catalyst]
X=Cl [*para*-Cl catalyst]

Fig. 1 Structure of 1,1′-ferrocenyldiacrylonitriles used as catalysts.

2. Results and discussion

2.1. Synthesis of para-CN, para-Cl and para-CF_3 catalysts

Synthesis of *para*-CN, *para*-Cl and *para*-CF_3 substituted catalysts was conducted as reported by Ombaka *et al.* [20]. Grinding together 1,1′-ferrocenedicarboxaldehyde and the substituted phenylacetonitriles in the presence of a drop of piperidine yielded the *para*-CN, *para*-Cl and *para*-CF_3 substituted catalysts as depicted in Scheme 1 [20]. The reaction mixture readily turned into a melt or a gum upon grinding at ambient temperatures. The obtained melt or gum was dried under vacuum and IR and ^{1}H-NMR spectroscopy were used to confirm the reaction completion.

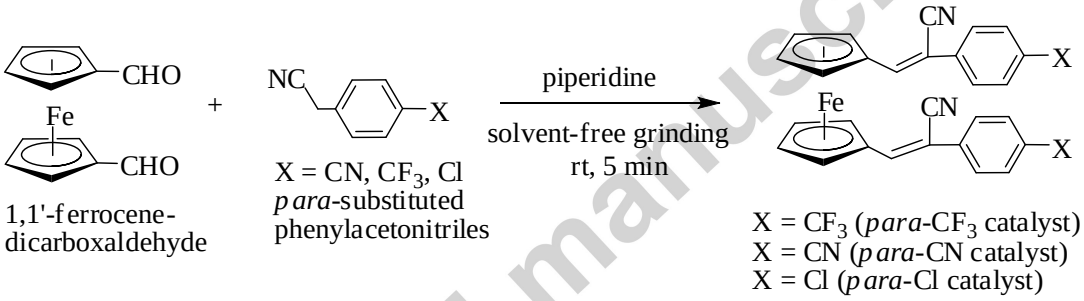

Scheme 1. Mechanochemical synthesis of 1,1′-ferrocenyldiacrylonitriles under solvent-free conditions.

2.1.1. Crystal structure of the para-CF_3 catalyst

We have previously reported the synthesis and characterization of the *para*-CF_3 catalyst [20], however, the crystal structure of this catalyst has not been reported. The molecular structure and atom numbering scheme of the *para*-CF_3 catalyst is presented in Fig. 2. Selected bond distances and angles of the *para*-CF_3 structure are summarized in Table 1. The crystal structure of the *para*-CF_3 catalyst contains a more bulky -CF_3 group on the *para*-position as opposed to the *para*-CN and *para*-Cl groups in the previously reported catalysts [20].

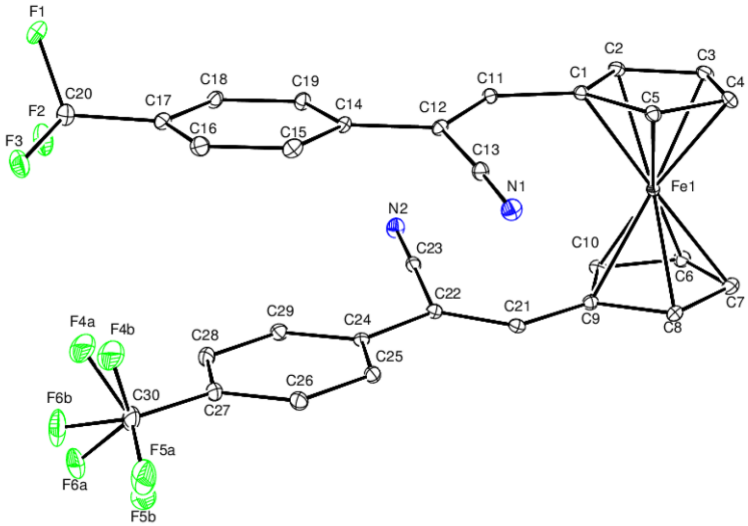

Fig. 2 ORTEP diagram for the para-CF_3 catalyst along with the atom-numbering scheme. The displacement ellipsoids are drawn at 50% probability level.

The bulky -CF_3 group does not seem to affect the arrangement of the two *para*-(trifluoromethyl)phenylacrylonitrile moieties since the structure adopts a *cisoidal* conformation which is observed in less bulky groups (*para* –CN and –Cl) that have been previously reported [20]. However, the two -CF_3 groups seem to influence the conformation around the C_{11}-C_{13} and C_{20}-C_{22} double bond in which the CN groups are observed to face opposite directions. The steric strain caused by the -CF_3 groups also tends to influence the cyclopentadienyl rings which are staggered by an angle of 17.9° from an ideal eclipsed geometry. The staggering angle in the *para*-CN and *para*-Cl were smaller (15.85° and 0.654°, respectively) [20].

All Fe-C bond distances and angles are well within the expected ranges of similar ferrocenyl derivatives [20]. In the *para*-CF_3 catalyst, the cyanoethyl benzonitrile groups are staggered by an angle of 170.5(4)° while, in the *para*-CN and -Cl catalysts the cyanoethyl benzonitrile groups were staggered by 165.86(18)° and 156.3(4)°, respectively [20]. As the *para*-substituent increases in size (*i.e.* Cl < CN < CF_3), the angle by which the cyanoethyl benzonitrile groups are staggered also increases. The increase in steric strain could be perpetuated by repulsive interactions between the two cyanoethyl benzonitrile groups resulting in a wider angle of staggering.

Table 1. Bond lengths [Å] and angles [°] for *para*-CF_3 catalyst.

C—C_{Cp}	1.442(5)	C—C_{Cp}	1.444(5)
C=C	1.355(5)	C=C	1.354(5)
C—C_{Ph}	1.480(5)	C—C_{Ph}	1.483(5)
C_{Cp}—C=C	130.4(3)	C_{Cp}—C=C	130.2(3)
C=C—C_{Ph}	124.2(3)	C=C—C_{Ph}	124.3(3)
C=C—C_N	119.8(3)	C=C—C_N	119.7(3)
C_{Ph}—*C*—C_N	116.0(3)	C_{Ph}—*C*—C_N	116.0(3)
C=C—C_{Ph}—C_{Ph}	170.5(4)	C=C—C_{Ph}—C_{Ph}	171.3(4)

2.2. Effect of the para-substituent and nitrogen source on SCNMs

In this section, the SCNMs synthesized by using the *para*-CF_3, -CN and -Cl catalysts are named as SCNMs-F, SCNMs-CN and SCNMs-Cl, respectively. In a similar manner, the N-CNTs obtained by use of *para*-CF_3, -CN and -Cl catalysts are named as N-CNTs-F, N-CNTs-CN, and N-CNTs-Cl, respectively.

Product yields obtained from all three catalysts dissolved in pyridine and acetonitrile are summarized in Table 2. Amongst the three catalysts used, the *para*-CF_3 catalyst gave the highest yield with pyridine or acetonitrile. The fluorine in *para*-CF_3 catalyst may have restructured the iron catalysts to a more active phase of higher carbon solubility hence increasing the yield of SCNMs [21]. The *para*-Cl catalysts gave the lowest yield with pyridine and acetonitrile. A previous report also observed that chlorinated catalysts lower the growth rate of SCNMs [22], this may be attributed to reactions between the catalysts active sites and chlorine which deactivate the catalysts thus decreasing the yield [23].

Table 2: Yield and product distribution of pristine SCNMs and amorphous carbon obtained by use of the three catalysts dissolved in pyridine or acetonitrile.

Catalyst	pyridine					acetonitrile				
	Yield (mg)	*N-CNTs (%)	H-N-CNTs (%)	CS (%)	A-c (%)	Yield (mg)	*N-CNTs (%)	H-N-CNTs (%)	CNFs (%)	A-c (%)
***Para*-CF_3**	256	10	70	13	7	30	20	60	-	20
***Para*-CN**	131	70	-	20	10	20	40	-	30	30
***Para*-Cl**	100	20	10	50	20	15	40	15	20	25

*N-CNTs: straight N-CNTs; A-c: amorphous carbon; H-N-CNTs: helical-N-CNTs; CS: carbonspheres

Higher yields were obtained with pyridine compared with acetonitrile, this is because pyridine has three extra carbon atoms thus, pyridine supplies higher quantities of carbon leading to greater yields of SCNMs [22]. Acetonitrile has a higher nitrogen:carbon ratio (1:2) than pyridine (1:5), the high nitrogen concentrations in acetonitrile slow down SCNMs growth rates thus lowering the yields [21].

TEM analysis on various images revealed that the nanotubes had bamboo compartments (see Fig. 3 a-c, and Fig. 4a-c) which is a characteristic trait associated with nitrogen-doped CNTs [24]. SCNMs obtained from pyridine and *para*-CF_3 or *para*-CN catalysts yielded N-CNTs as the main product, whilst the use of the *para*-Cl catalyst in pyridine yields mainly CS (Table 2). When acetonitrile is used as a carbon/nitrogen source, N-CNTs are still produced as the major product but the minor product changes to CNFs (Fig. 4 and Table 2).

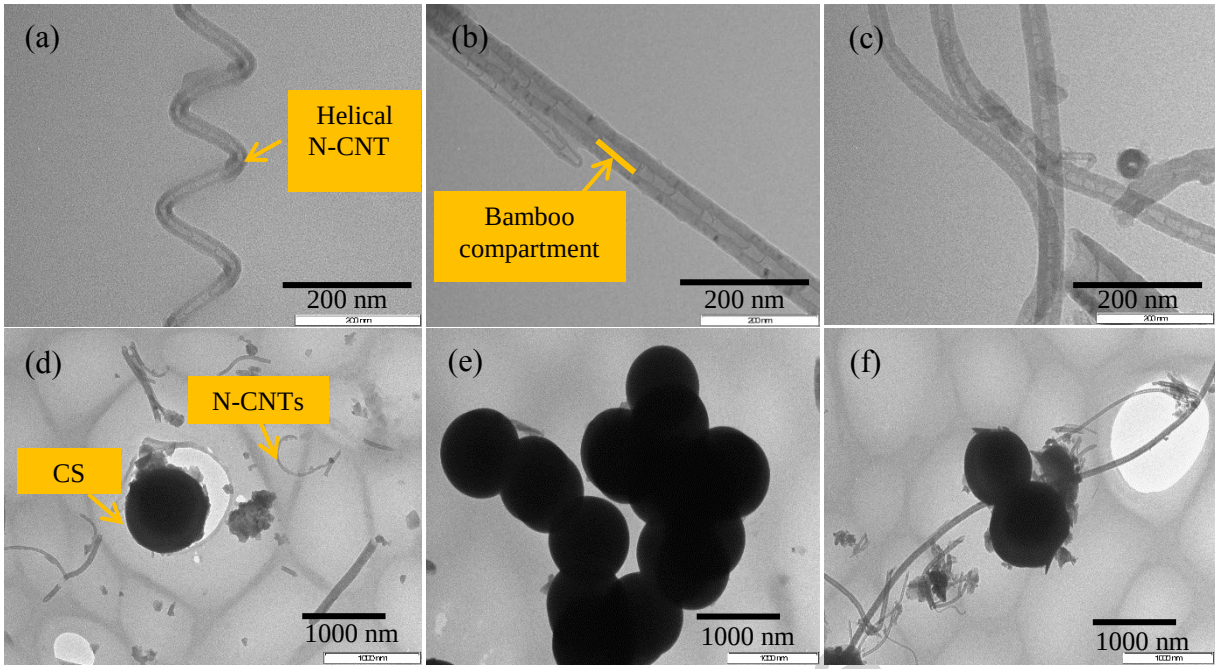

Fig. 3 TEM images of pristine N-CNTs synthesized by use of (a) para-CF_3, (b) para-Cl and (c) para-CN catalysts, and TEM images of N-CNTs and CS synthesized by using (d) para-CF_3, (e) para-Cl and (f) para-CN catalysts in pyridine.

N-CNTs synthesized with the *para*-CF_3 catalyst in pyridine are predominantly helical (Fig. 3a and Supplementary data S1). Helical-CNTs (H-CNTs) have been reported to favourably grow over small (15-30 nm) iron catalyst particles [25] which facilitate formation of pentagonal and heptagonal structures that lead to kinks in the CNTs [22]. The fluorine atoms present in the *para*-CF_3 catalyst may have reduced the diameter of iron catalyst to a size which increases the selectively towards the growth of H-N-CNTs.

The *para*-Cl catalyst yields the highest quantity of CS while the *para*-CF_3 catalyst gives the least amount of CS (Table 2). This can be attributed to the fact that fluorine, just like oxygen can act as an oxidising agent that 'cleans out' dangling carbon atoms, which prevalently form CS, and in the process reduces the formation of CS. On the contrary, the *para*-Cl moiety seems to have poisoned the iron nanoparticle catalysts to favour formation of CS [26]. These observations contradict the report of Lv *et al*. [13] who observed good CNTs yield with chlorinated synthesis precursors.

The use of *para*-CF_3, and acetonitrile, yields N-CNTs as the only SCNMs, while use of *para*-CN and *para*-Cl yields a mixture N-CNTs and CNFs (Table 2 and Fig. 4). The para-Cl in

acetonitrile gave higher percentages of N-CNTs than in pyridine (Table 2). The formation of CNFs can be correlated with the abundance of reactive hydrogen radicals emanating from the catalyst during synthesis [27]. The molecular hydrogen pumped through the reaction chamber reduces Fe^{2+} species to Fe^{0} that catalyses SCNM growth [28], but the reactive hydrogen radicals enhance CNF formation [29]. During synthesis, chlorine and fluorine heteroatoms, present in the *para*-CF_3 and -Cl catalysts, can react with such reactive hydrogen radicals, thereby reducing their abundance and promoting formation of N-CNTs.

TEM images of N-CNTs synthesized from the *para*-CF_3 and -Cl catalysts in acetonitrile exhibited bamboo compartments and encapsulated iron nanoparticles in the N-CNTs cavities (Figures 3b and c). N-CNTs-F show more iron encapsulation than N-CNTs-Cl, while N-CNTs-CN did not show any iron encapsulation indicating that chlorine and fluorine heteroatoms aided the formation of iron-encapsulated N-CNTs. In a similar manner, Lv *et al*. synthesized metal-filled CNTs by use of chlorine-substituted benzene [13] and ferrocene catalysts. No iron encapsulation was observed in N-CNTs obtained from pyridine, this may imply that the ratio of carbon: halogen influences the encapsulation of iron.

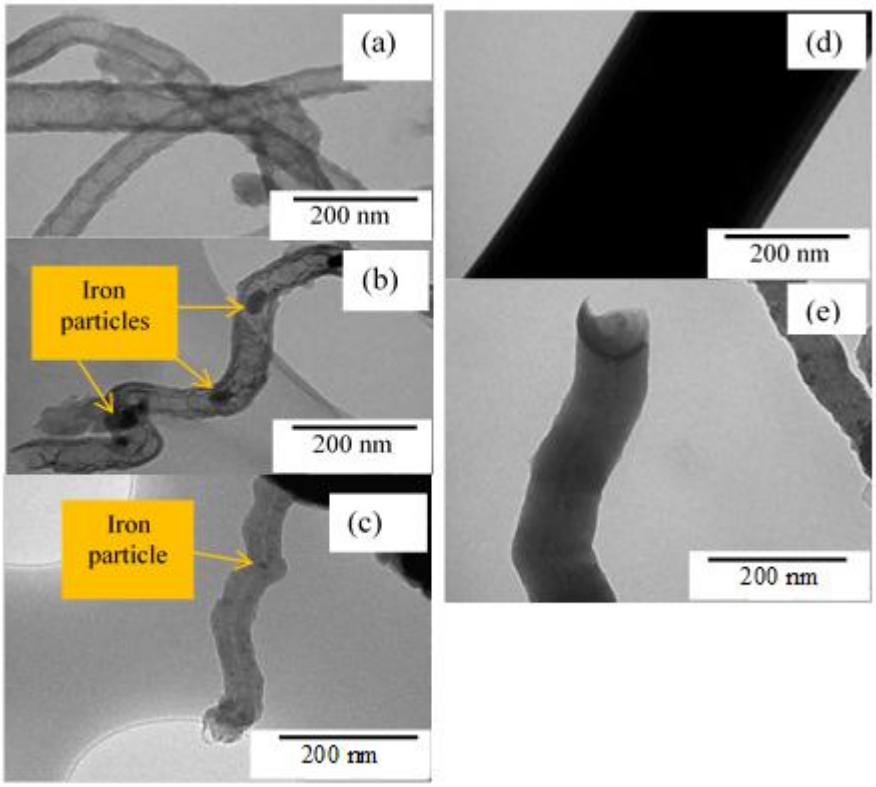

Fig. 4 TEM images of pristine N-CNTs synthesized by using (a) para-CN, (b) para-CF_3 and (c) para-Cl catalyst in acetonitrile. TEM images of CNFs synthesized by use of (d) para-CN and (e) para-Cl catalyst in acetonitrile.

The outer and inner diameters (OD and ID, respectively) of all N-CNTs (Fig. 5) have been obtained from analysis of the TEM images. The diameters of N-CNTs obtained with pyridine are generally smaller than those obtained with acetonitrile as a nitrogen source. The OD and ID of N-CNTs synthesized using all three catalysts, in pyridine, showed no significant difference as opposed to those synthesized using the *para*-CF_3 and -Cl catalysts, in acetonitrile, which exhibited reduced OD and ID compared to when *para*-CN catalyst was used.

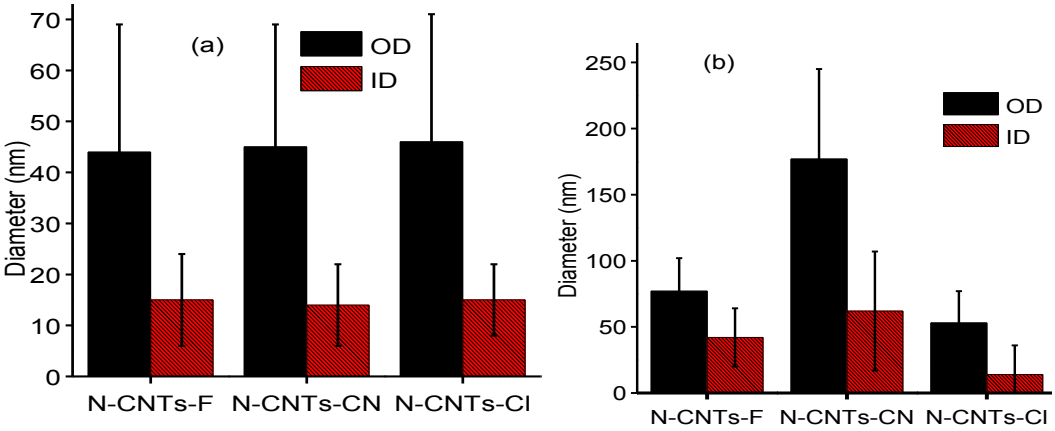

Fig. 5 Outer diameter (OD) and inner diameter (ID) of pristine N-CNTs synthesized by using the para-CF_3, para-CN and para-Cl catalysts in (a) pyridine and (b) acetonitrile.

Pyridine was a better carbon source than acetonitrile because it gave higher yields of SCNMs with all catalysts (Table 2). Hence, further characterization of SCNMs by use of Raman spectroscopy, TGA, FTIR and XPS were only conducted on the products obtained from pyridine.

2.2.1. Crystallinity of SCNMs

Raman spectroscopy was used to evaluate the crystallinity of SCNMs synthesized from all three catalysts in pyridine (Fig. 6a). From the Raman spectra, two first-order peaks, i.e. a disorder band (D-band) at 1376-1399 cm^{-1} and a graphitic band (G-band) at 1569-1604 cm^{-1} are observed [30]. The D-band is due to the breathing modes of disordered sp^2 hybridized carbons, while the G-band is caused by the stretching modes of sp^2 hybridized graphitic carbon networks [31]. An increase of disorder in the graphene structures results in a more intense D-band than the G-band, and *vice-versa* for a decrease in disorder. Thus, the Tuinstra-Koening relationship I_D/I_G (integrated area of the D-band:integrated area of the G-band) has been applied to determine the crystalline nature of SCNMs [32, 33]. A lower I_D/I_G ratio indicate a higher degree of crystallinity, while a higher I_D/I_G ratio imply the reverse.

SCNMs-F exhibit the lowest value of I_D/I_G while SCNMs-Cl have the highest I_D/I_G value (Fig. 6b). The higher I_D/I_G value observed from SCNMs-Cl is indicative of the presence of more amorphous carbons [34] or CS in these samples because amorphous carbons are normally inherently disordered giving rise to a strong D-band intensity [35]. This observation supports the greater quantity of amorphous carbon and CS observed from TEM analysis of SCNMs-Cl (Table

2). Likewise, the lower I_D/I_G value of SCNMs-F corresponds with the lower percentage of amorphous carbons in these samples as observed from the TEM analysis (Table 2). Generally, the I_D/I_G ratio correlated directly with the quantity of amorphous carbon in the SCNMs.

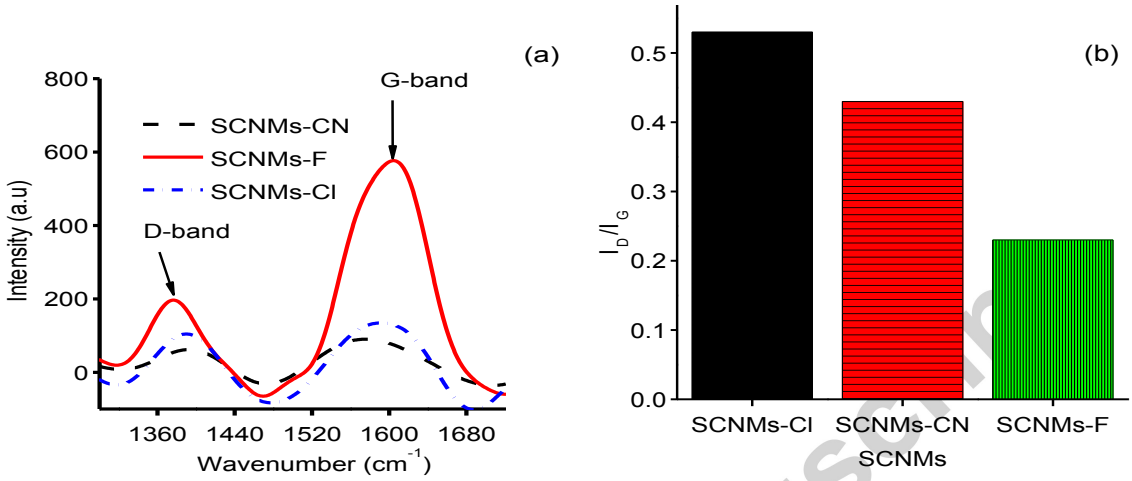

Fig. 6 (a) Raman spectra and (b) I_D/I_G ratio of pristine SCNMs synthesized by use of para-CF_3, para-CN and para-Cl catalysts in pyridine.

The G-band seems to shift from 1592 cm^{-1} (SCNMs-Cl) to 1604 cm^{-1} (SCNMs-F). This shift may be attributed to the reduction of the in-plane correlation length in ordered graphene sheets [30] caused by nitrogen-doping. It is also important to note that the D- and G-bands of SCNMs-F exhibit a much greater intensity than those of other samples (Fig. 6a). Similar observations were made from the Raman spectra of N-CNTs synthesized with 4 wt.% oxygen in acetonitrile [8]. Since fluorine neighbours oxygen in the periodic table, it is possible that fluorine just like oxygen can etch the walls of N-CNTs thus increasing the Raman intensity [36].

2.2.2. Thermal stability of SCNMs

TGA analyses were used to determine the thermal stability of SCNMs synthesized by use of all three catalysts in pyridine. The thermograms and derivative thermograms (DTG) are presented in Fig. 7. From the thermograms (Fig. 7a) it is evident that SCNMs-F are the least thermally stable while SCNMs-Cl and -CN exhibit a similar thermal stability. The lower decomposition temperature of SCNMs-F can be associated with the increased number of H-N-CNTs observed from TEM images of these samples. These H-N-CNTs have a higher density of defects than straight N-CNTs which results in a lowering of the decomposition temperature [37].

The observed lower thermal stability of SCNMs-F parallels the observation made from TGA analysis of N-CNTs synthesized by using 4 wt.% oxygen in acetonitrile [8]. Thus, it is likely that fluorine, just like oxygen, enhances defects in N-CNTs thus decreasing the sample thermal stability. Between 800-1000 °C, the residual weight on all curves increases due to oxidation of iron to iron oxide (Fig. 7a).

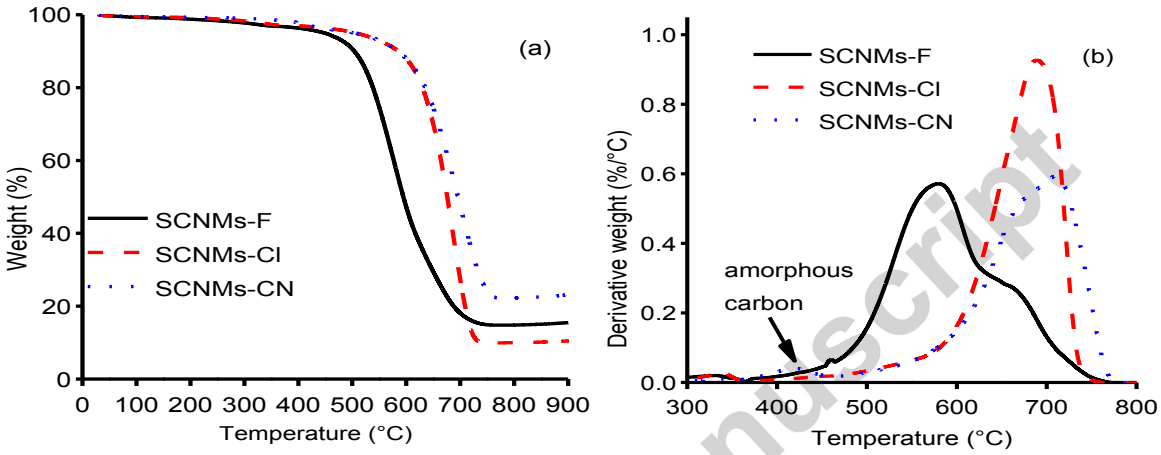

Fig. 7 (a) Thermograms and (b) derivative thermograms (DTG) of pristine SCNMs synthesized by using para-CF_3, para-CN and para-Cl catalysts in pyridine.

The DTG of all SCNMs showed a minor peak (≈350-450 °C) and a broad major peak (≈500-800 °C). The minor peak is associated with amorphous carbon present in all samples as observed from TEM analysis. The major peak arises from the overlap of the decomposition peaks of N-CNTs and CS. The peak corresponding to SCNMs-F significantly differs from those of SCNMs-CN and SCNMs-Cl in terms of shape and position. This can be due to the presence of more oxygen functionalities or the incorporation of a pyridinic nitrogen species in the N-CNTs-F, as mentioned in Section 2.2.3 [36]. The oxygen or nitrogen species may have increased the number impurities in N-CNTs-F leading to an overall decrease in thermal stability of N-CNTs-F [38]. A similar trend in DTG curves is also observed in the DTG of N-CNTs synthesized by use of 4 wt.% oxygen in acetonitrile [8]. The DTG curve for SCNMs-Cl is narrower and sharper than that of SCNMs-F and SCNMs-CN indicating that this sample is more homogeneous than the other two samples.

2.2.3. Surface chemistry of N-CNTs and CS

FTIR spectroscopy and XPS analysis were used to analyse the surface chemistry of the SCNMs synthesized by use of all three catalysts in pyridine (Fig. 8). A broad band appearing at ≈3400 cm^{-1} is observed in the spectra of all samples and is assigned to the stretching vibrations of -OH groups in water molecules adsorbed onto the SCNMs [39]. The transmittance peaks at ≈2950-2850 cm^{-1} correspond with the stretching vibration of dangling CH_2 and CH_3 groups attached to the aromatic rings of graphene and amorphous carbons [40]. The stretching vibrations of CO_2 groups arising from the single beam FTIR spectrometer are observed at ≈2381 cm^{-1} [41]. The stretching modes of the C=C bonds found in the aromatic rings of CNTs are observed at 1678 cm^{-1}, while the C-H vibration modes are observed at 788 and 699 cm^{-1} [40].

The stretching vibrations of C=N that have been reported to appear at ≈1567 cm^{-1} [41-44] appear to have overlapped with the C=C stretching modes to form a broad peak between 1519-1713 cm^{-1}. This peak is most prominent and intense in SCNMs-F and SCNMs-Cl compared with SCNMs-CN. Therefore, it is possible that there is more nitrogen-doping in N-CNTs-F and N-CNTs-Cl than in N-CNTs-CN. This possibility is further supported by the lower thermal stability of these samples observed from TGA analysis [45].

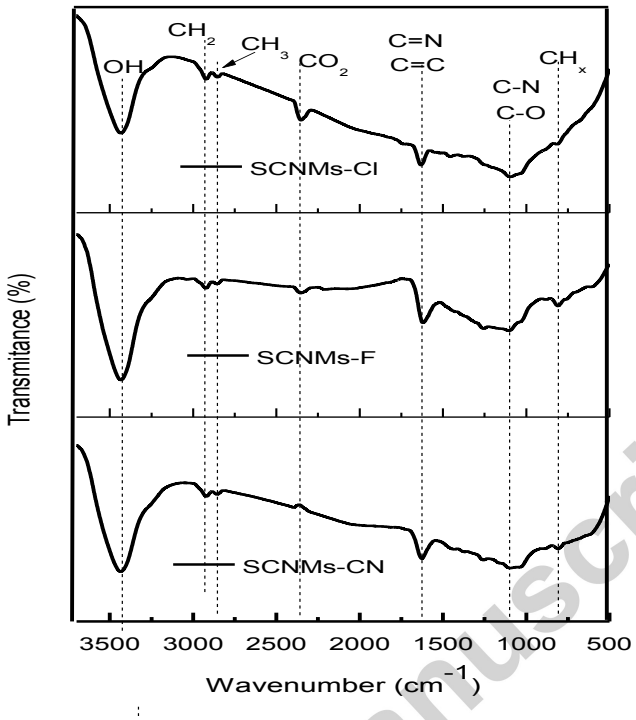

Fig. 8 FTIR spectra of pristine SCNMs synthesized by using para-CF_3, para-CN and para-Cl catalysts in pyridine.

Elemental analysis of the SCNMs was obtained by the use of XPS. From XPS analysis, chlorine was not detected in SCNMs-Cl, neither was fluorine detected in SCNMs-F, and this was affirmed by the EDX and XPS analysis. This observation differed from the report of Gui *et al*. who observed low concentration of Cl in CNTs synthesized from ferrocene and dichlorobenzene as a source of chlorine [14]. Thus, the use of halogenated ferrocenyl derivatives may have the advantage of eliminating halogen-functionalization of N-CNTs thus yielding more pure products. The data obtained from XPS analysis showed that nitrogen (3.65-4.05 wt.%) was present in all SCNMs (Table 3). Similar levels of nitrogen-doping were present in SCNMs-F and SCNMs-Cl. SCNMs-CN showed the least amount of nitrogen doping despite having two extra nitrogen atoms on the structure of the *para*-CN catalyst, suggesting that the generated nitrogen species do not necessarily favour nitrogen-doping. Since SCNMs-F and SCNMs-Cl have an almost equal nitrogen content, it is expected that their thermal decomposition temperature would be almost equal. However, this is not the case as SCNMs-F are less thermally stable than SCNMs-Cl (Fig. 7). The decrease in thermal instability of SCNMs-F was attributed to the presence of higher oxygen levels in these samples (Table 3). In general, both fluorine and chlorine enhances the

nitrogen-doping of N-CNTs. The binding energy of nitrogen or carbon to the catalytic metal nanoparticle influences the properties of the obtained N-CNTs [46]. Thus, it is possible that fluorine and chlorine heteroatoms increase the binding energy between nitrogen and iron catalyst resulting in higher nitrogen-doping levels in SCNMs-F and -Cl.

Table 3: Nitrogen content and species in pristine SCNMs synthesized by use of *para*-CF_3, *para*-CN, *para*-Cl and ferrocene catalysts in pyridine.

	O_2 %	N at. %	Composition (%) of N species			
Catalyst			N1	N2	N3	N4
para-CF_3	14.4	4.05	35.1	44.7	9.6	10.8
para-Cl	11.4	4.04	36.3	43.0	8.3	12.5
para-CN	11.0	3.65	29.3	44.9	14.7	11.1

For comparison purposes, the nitrogen-content of SCNMs synthesized by use of ferrocene catalyst in pyridine was evaluated. SCNMs obtained with ferrocene had a nitrogen content of 2.18 wt.% which was lower than that in SCNMs obtained by using *para*-CF_3, *para*-Cl and *para*-CN catalysts (3.65-4.05 wt.%). Thus, the use of nitrogen and halogen-containing ferrocenyl derivatives as catalysts in the synthesis of SCNMs increases nitrogen-doping compared with the use of ferrocene. The nitrogen content in SCNMs obtained with the halogenated ferrocenyl catalysts was comparable to that in previous reports [9, 28]. During synthesis, just like oxygen, fluorine and chlorine are reactive elements that can induce defects in the graphitic structure of CNTs [8]. Defective carbon structures are more reactive than their graphitic counterparts, thus, they readily accept the incorporation of heteroatoms such as nitrogen species into their structure [47]. Consequently, fluorine and chlorine in the halogenated catalysts may have enhanced nitrogen-doping levels *via* defects.

The N 1s spectra of all SCNMs showed overlapped peaks between 399.0–405.9 eV that were deconvoluted into four nitrogen (N1, N2, N3 and N4) species (Fig. 9 and Table 3). The lowest energy peak appeared at 399.0 eV, this peak was labelled N1 and assigned to pyridinic nitrogen species [48, 49]. The next peak labelled as N2 appeared at 400.7 eV, was attributed to pyrrole nitrogen species [50]. The third peak having an energy of 402.5 eV was coded N3, this peak was accredited to quaternary amine [51]. The fourth peak, which appeared at 405.9 eV was coded N4 and attributed to nitrogen molecules adsorbed or encapsulated within the graphene layers of

SCNMs [52].

Interestingly, SCNMs-F and SCNMs-Cl exhibited a higher quantity of pyridinic nitrogen (N1) than SCNMs-CN (Table 3). On the other hand, SCNMs-CN had a higher composition of quaternary amine (N3) compared to SCNMs-F and SCNMs-Cl. Thus, the halogen *para*-substituents promoted pyridinic nitrogen-doping at the expense of quaternary amine nitrogen-doping. The higher quantity of pyridinic nitrogen species in SCNMs-F and -Cl may have led to the decrease in the thermostability of these samples (Fig. 7).

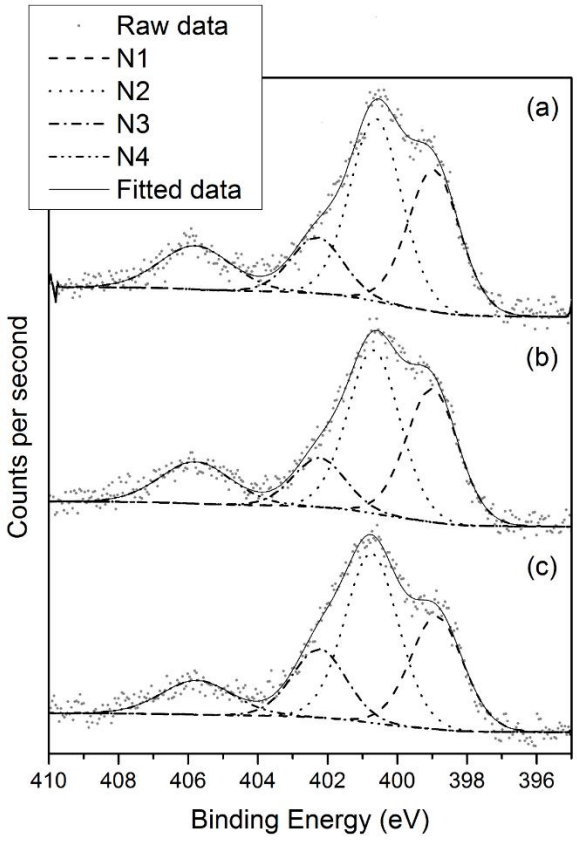

Fig. 9 XPS high resolution N 1s envelopes of SCNMs synthesized by use of (a) para CF_3, (b) para-Cl and (c) para-CN.

3. Conclusions

1,1′-Ferrocenyldiacrylonitriles were synthesized *via* a solvent-free approach and the X-ray crystallographic structure of 1,1′-ferrocenyldi[-2(4-{trifluoromethyl}phenyl)acrylonitrile] is reported for the first time. From the crystallographic studies, it is apparent that the structures of the three catalysts are influenced by the size of the *para*-substituent.

N-CNTs were successfully synthesized by use of 1,1′-ferrocenyldiacrylonitriles as catalysts in either pyridine or acetonitrile as both the nitrogen and carbon source. The use of pyridine yielded N-CNTs as the major SCNM product and CS as the minor product. The use of acetonitrile gave N-CNTs as the major SCNM and CNFs as the minor product. The yields obtained with pyridine were generally higher that those obtained with acetonitrile.

Amongst the three catalyst used (i.e. *para*-CF_3, *para*-Cl and *para*-CN), the *para*-CF_3 catalyst was most efficient for the synthesis of high percentages of N-CNTs in pyridine and acetonitrile. The morphology and surface chemistry of N-CNTs synthesized by use of pyridine and the *para*-CF_3 or *para*-Cl catalyst significantly differed from that of the *para*-CN catalysts with pyridine as they were helical and had a higher nitrogen content. This implied that fluorine and chlorine, just like oxygen, modulates the morphology of N-CNTs and the nitrogen content and species incorporated into N-CNTs.

The halogenated catalysts in acetonitrile promoted iron filling of N-CNTs and reduced the diameters of N-CNTs while decreasing the abundance of CNFs. On the other hand, no significant difference was observed in the tube diameters of N-CNTs obtained by use of pyridine and the three catalysts. This implied that the effect of halogens on tube diameters is dependent on the carbon: halogen ratio. Further analysis is required to provide a plausible mechanism on how the halogens enhances the nitrogen-doping.

4. Experimental Section

4.1. Materials and characterization

All chemicals and solvents used were of analytical grade and were used as received. Aluminium-backed silica gel 60 F_{254} plates were used to carry out thin layer chromatography in

solvents of varying polarity. Purification of products by column chromatography was accomplished by using silica gel 60, 0.063-0.2 mm. The melting points of various compounds were determined either by using a Bibby Stuart Scientific model SMP3 apparatus or by use of a Shimadzu Differential Scanning Calorimeter (DSC 60) apparatus. Infrared spectroscopy was conducted on a Perkin Elmer Universal 100 FTIR spectrometer equipped with an ATR accessory. The ^{1}H- and ^{13}C-NMR spectra were recorded on a 400 MHz Bruker Ultrashield spectrometer at room temperature. For NMR spectroscopy analysis, samples were dissolved in deuterated chloroform and values were obtained relative to tetramethylsilane. Mass spectra of various compounds were obtained from a mass spectrometry (MS) with an electrospray ionization (ESI).

For synthesis of N-CNTs, acetonitrile 99.9% and pyridine 99.8% were purchased from LiChroSolv, Germany. N-CNTs were synthesized in a quartz tube reactor (inner diameter 27 mm, length 850 mm) which was placed in a muffle furnace (Elite Thermal Systems Limited Model No. TSH12/50/610). The carrier gas used during synthesis of N-CNTs was 10% hydrogen in argon (v/v) purchased from Airflex Industrial Gases, South Africa. The rate of injection was controlled by a syringe pump (model no. NE-300, New Era Pump Systems Inc.). Images of N-CNTs were taken by use of a transmission electron microscope (TEM) (JEOL JEM 1010). The graphitic natures of N-CNTs were determined with Raman spectrometer (DeltaNu Advantage 532™). The thermo-stability of N-CNTs was studied by using a TA Instrument Q Series™ Thermal Analyzer DSC/TGA (Q600). Infrared spectra of N-CNTs embedded into KBr pellets were recorded on a Perkin Elmer Spectrum RX1 FTIR spectrometer. Elemental analysis of N-CNTs was performed on a LECO CHNS-932 elemental analyzer, standardized with acetanilide. X-Ray Photoelectron Spectroscopy (XPS) analysis was conducted on a Kratos Axis Supra instrument using a monochromated Al Kα source and charge neutraliser. High resolution data was collected with a pass energy of 20 eV, and the peaks deconvoluted using the CasaXPS program.

4.2. General procedure for synthesis of 1,1'-ferrocenyldiacrylonitrile

The general procedure for the synthesis and characterization of 1,1′-ferrocenyl-diacrylonitriles is displayed in Scheme 1 and has been previously reported [20]. In brief, 1,1′-

ferrocenedicarboxaldehyde and substituted phenylacetonitriles (2.2 eq.) were mixed in a Pyrex tube fitted with a ground glass joint. The compounds were thoroughly ground in the open air with a glass rod in the presence of 1-2 drops of piperidine to form a melt. The melt was first dried in open air, followed by drying under a vacuum line. The dry products were purified by means of silica gel chromatography. Formation of the products was determined by use of IR or NMR spectroscopy (^{1}H- and ^{13}C-NMR). In the solid-state IR spectra, the formation of the products was characterized by the disappearance of the sharp carbonyl absorption band at approximately 1650 cm^{-1} and the appearance of a strong nitrile absorption band at approximately 2200 cm^{-1}. The ^{1}H- and ^{13}C-NMR spectra showed the disappearance of the carbonyl resonance (≈10 ppm) and the appearance of alkene resonance peaks (≈7.4 ppm). Pure compounds were further analysed by melting point determination (DSC), mass spectrometry, microanalysis, and X-ray diffraction.

4.2.1. 1,1′-Ferrocenyldi[-2(4-cyanophenyl)acrylonitrile] (para-CN catalyst)

The general procedure for the synthesis of this catalyst is described in Section 4.2 and involves the use of 1,1′-ferrocenyldicarboxaldehyde (145.0 mg, 0.60 mmol) and 4-cyanophenylacetonitrile (188.0 mg, 1.32 mmol). Upon grinding, a deep maroon paste was formed which was dried to obtain a maroon solid. Reaction completion was monitored by use of preparative TLC plates with a solvent system of hexane/diethyl ether (1:1). The final product was then purified by means of column chromatography with a solvent system of hexane/diethyl ether (1:1) to obtain dark maroon crystals (219.0 mg, 74%) as the desired product and 37.0 mg of the recovered starting (1,1′-ferrocenedicarboxaldehyde). Product d.p. *ca*. 325 °C; IR (cm^{-1}) 3182, 2926, 2852, 2213, 1608, 1587, 1510, 1452, 1417, 1371, 1319, 1251, 1180, 1035, 996, 918, 830, 819, 542, 501, 486, 456, 425; ^{1}H-NMR spectra ($CDCl_3$) 7.55 (4H, d, *J* 8.4 Hz, ArH), 7.47 (4H, d, *J* 8.5 Hz, ArH), 7.34 (2H, s, CH), 5.08 (4H, s, C_5H_4), 4.65 (4H, s, C_5H_4); ^{13}C-NMR spectra ($CDCl_3$) 132.7, 125.3, 77.2, 73.7, 72.2; HR-MS ($C_{30}H_{18}FeN_4$) ES: [M + H^+] *m/z* calc. 491.0959, found 491.0969.

4.2.2. 1,1′-Ferrocenyldi[-2(4-chlorophenyl)acrylonitrile] (para-Cl catalyst)

The general procedure for synthesis of this catalyst is described in Section 4.2 and involves the use of 1,1′-ferrocenyldicarboxaldehyde (145.0 mg, 0.60 mmol) and 4-chlorophenylacetonitrile (200.0 mg, 1.32 mmol). Upon grinding the two substances in the presence of a drop of piperidine (0.05 ml), the solid mixture transformed into a brown paste, which eventually turned into a red solid. The reaction completion was monitored by using preparative TLC plates with a solvent system of hexane/dichloromethane (1:1). The red paste was dried, then purified by means of column chromatography in hexane and dichloromethane (1:1) solution to obtain the product as a red solid and 87.0 mg of the recovered starting 1,1′-ferrocenedicarboxaldehyde. Characterization of the red solid gave the *para*-Cl catalysts (153.0 mg, 52%) m.p. 238 °C; IR (cm^{-1}) 3087, 3050, 2209, 1898, 1649, 1598, 1493, 1456, 1411, 1374, 1329, 1305, 1251, 1186, 1094, 1037, 997, 917, 827, 815, 774, 745, 540, 499, 489, 437, 396; ^{1}H-NMR spectra ($CDCl_3$) 7.22 (4H, s, ArH), 7.18 (4H, s, ArH), 7.15 (2H, s, CH), 5.06 (4H, s, C_5H_4), 4.56 (4H, s, C_5H_4); ^{13}C-NMR spectra ($CDCl_3$) 140.1, 129.1, 126.0, 79.3, 72.7, 71.5; HR-MS ($C_{28}H_{18}Cl_2FeN_2$) ES: $[M]^+$ *m/z* calc. 508.0196, found 508.0199.

4.2.3 1,1′-Ferrocenyldi[-2(4-{trifluoromethyl}phenyl)acrylonitrile] (para-CF_3 catalyst)

The general procedure for synthesis of this catalyst is described in Section 4.2 and involves the use of 1,1′-ferrocenyldicarboxaldehyde (145.0 mg, 0.60 mmol) and 4-(trifluoromethyl)phenylacetonitrile (244.0 mg, 1.32 mmol). Upon grinding a deep red paste was formed, which was dried to obtain a red solid. The reaction completion was monitored by use of preparative TLC plates with a solvent system of hexane/diethyl ether (1:1) and the product was then purified by means of column chromatography with a solvent system of hexane/diethyl ether (1:1) to obtain red crystals as the product (268.0 mg, 78%) and 31.0 mg of the recovered starting 1,1′-ferrocenedicarboxaldehyde. Product m.p. 252 °C; IR (cm^{-1}) 3059, 2924, 2216, 1617, 1593, 1456, 1421, 1324, 1255, 1157, 1111, 1070, 1000, 925, 824, 729, 667, 642, 621, 584, 477, 421; ^{1}H-NMR spectra ($CDCl_3$) 7.40 (8H, q, *J* 5 Hz, ArH), 7.31 (2H, s, CH), 5.12 (4H, s, C_5H_4), 4.62 (4H, s, C_5H_4); ^{13}C-NMR spectra ($CDCl_3$) 141.4, 125.9, 124.8, 107.3, 79.1, 77.2, 73.1, 72.9; HR-MS ($C_{30}H_{18}F_6FeN_2$) ES: $[M]^+$ *m/z* calc. 576.0724, found 576.0717.

4.2.3.1. X-ray crystallography analysis of the para-CF_3 catalyst

Crystal evaluation and data collection for the *para*-CF_3 catalyst was performed on a Bruker Smart *APEXII* diffractometer with Mo Kα radiation (λ = 0.71073 Å) and a diffractometer to crystal distance of 4.00 cm. The initial cell matrix was obtained from three series of scans at different starting angles. Each series consisted of 12 frames collected at intervals of 0.5° in a 6° range with the exposure time of about 10 seconds per frame. The reflections were successfully indexed by an automated indexing routine built in the *APEXII* program suite [53]. Data collection method involved ω scans of width 0.5°. Data reduction was carried out by means of the program *SAINT+* and *XPREP* [53] while the structure was solved and refined by using the *SHELXL* [54]. H-atoms were added geometrically and fixed during refinement for all concerning atoms. *WinGX* [55] and *ORTEP3* [56] were used to prepare molecular graphics and material for publication [54]. The crystal data and structure refinement information for the *para*-CF_3 catalyst are summarized in Table 4.

Disorder was found for one trifluoromethyl F-atoms, which is not an uncommon situation. The disorder was modelled for F atoms using distance restraints, displacement parameters restraints and PART instructions while keeping the total occupancy at each atom site as 1 during the refinement. All fluorine atoms involved in the disorder were modelled with anisotropic thermal parameters.

Table 4. Crystal data and structure refinement for the *para*-CF_3 catalyst.

Empirical formula	C_{30} H_{18} F_6 Fe N_2
Formula weight	576.31
Temperature (K)	173(2)
Wavelength (Å)	0.71073
Crystal system	Triclinic
Space group	$P\bar{1}$
Unit cell dimensions (Å/°)	
a, *α*	7.3569(3), 78.379(2)
b, *β*	11.7726(4), 87.424(2)
c, *γ*	14.2107(5), 86.612(2)
V (Å^3)	1202.76(8)
Z	2
σ (Mg/m^3)	1.591
μ (mm^{-1})	0.697
F(000)	584
Crystal size (mm^3)	0.450 x 0.090 x 0.090
θ range (°)	1.768 to 28.320.
Index ranges	$-9 \leq h \leq 9$, $-15 \leq k \leq 15$, $-18 \leq l \leq 18$
Reflections ions collected	30003
Independent reflections	5945 [R(int) = 0.0326]
Completeness to *θ*	99.7 % (25.242°)
Absorption correction	Semi-empirical from equivalents
Max. and min. transmission	0.939 & 0.731
Refinement	Full-matrix least-squares on F^2
Data/restraints/parameters	5945/114/380
GOOF on F^2	1.113
Final R indices [I>2sigma(I)]	R1 = 0.0699, *w*R2 = 0.1778
R indices (all data)	R1 = 0.0707, *w*R2 = 0.1782
Largest diff. peak and hole (e.Å^{-3})	1.881 &.977

4.3. Synthesis of N-CNTs

N-CNTs were synthesized by using a chemical vapour deposition (CVD) technique as outlined by Ombaka *et al*. [8] and Oosthuizen *et al*. [57]. In brief, three ferrocenyl-diacrylonitriles with substituted *para*-CF_3, -CN or -Cl (Fig. 1) were used as catalysts. Acetonitrile or pyridine was used as the main nitrogen and carbon source. A solution made by dissolving 0.25 g of the catalyst in 9.75 g of either acetonitrile or pyridine (i.e. 2.5 wt.% of catalyst) was made and used to synthesize N-CNTs.

The solution of synthesis precursors was injected at a flow rate of 0.8 mL min^{-1} into a quartz tube placed in a muffle furnace. The synthesis precursors were carried through the quartz tube by a carrier gas (10% hydrogen in argon (v/v)), which was pumped at a rate of 100 mL min^{-1} at 80 kPa. A reaction temperature of 850 °C was used for all experiments and, the furnace was set to maintain this temperature for 30 minutes during synthesis. Upon completion of the reaction, the reactor was left to cool to room temperature and the products formed were collected from the hot zone of the quartz tube.

Supplementary data

Supplementary data S1 displays addition TEM images of N-CNTs synthesized from the the fluorinated catalyst. Crystallographic data in *cif* format have been deposited with the Cambridge Crystallographic Data Centre (CCDC) as supplementary material for this paper. The CCDC number is 1419746 for *para*-CF_3 catalyst. These data can be obtained free of charge via www.ccdc.cam.ac.uk/conts/retrieving.html or from the CCDC, 12 Union Road, Cambridge CB2 1EZ, UK; fax: +44 1223 336033 or e-mail: deposit@ccdc.cam.ac.uk.

Acknowledgments

This research was financed by the National Research Foundation (NRF) and University of KwaZulu-Natal (UKZN). Lucy M. Ombaka is grateful for the award of doctoral bursary from the UKZN, collage of Agriculture, Engineering and Science. We are grateful to Prof B. S. Martincigh for assisting in proofreading the manuscript and her critical comments of the manuscript. We are also grateful to Ms. T. A. Ntshele for assisting with purification of the catalysts. J.D. McGettrick and M.L. Davies would like to thank the EPSRC and Innovate UK for the SPECIFIC Innovation and Knowledge Centre (grant numbers EP/I019278/1, EP/K000292/1, EP/L010372/1) and the Welsh Government for support to the Sêr Solar program.

References

[1] L. M. Ombaka, P. Ndungu, V. O. Nyamori, Catal. Today 217 (2013) 65.

[2] H. Dai, Nanotube growth and characterization, in: M.S. Dresselhaus, G. Dresselhaus (Eds.), Carbon Nanotubes Synthesis, Structure, Properties and Applications, Springler-Verlag, Heidelberg, 2001, pp. 29.

[3] R. Yuge, K. Toyama, T. Ichihashi, T. Ohkawa, Y. Aoki, T. Manako, Appl. Surf. Sci. 258 (2012) 6958.

[4] J. J. Niu, J.N. Wang, Y. Jiang, L. F. Su, J. Ma, Microporous and Mesoporous Mater. 100 (2007) 1

[5] G. Wang, Y. Ling, F. Qian, X. Yang, X.-X. Liu, Y. Li, J. of Power Sources 196 (2011) 5209.

[6] W. J. Lee, U. N. Maiti, J. M. Lee, J. Lim, T. H. Han, S. O. Kim, Chem.Commun. 50 (2014) 6818.

[7] M. I. Ionescu, Y. Zhang, R. Li, H. Abou-Rachid, X. Sun, Appl. Surf. Sci. 258 (2012) 4563.

[8] L. M. Ombaka, P. G. Ndungu, V. O. Nyamori, J. Mater. Sci. 50 (2015) 1187.

[9] P. Chen, F. Yang, A. Kostka, W. Xia, ACS Catal. 4 (2014) 1478.

[10] B. Padya, D. Kalita, P. K. Jain, G. Padmanabham, M. Ravi, K. S. Bhat, J. Nanoelectron. Optoe. 8 (2013) 177.

[11] R. C. Che, L. M. Peng, X. F. Duan, Q. Chen, X. L. Liang, Adv. Mater. 16 (2004) 401.

[12] S. Liu, X. Tang, Y. Mastai, I. Felnerc, A. Gedanken, J. Mater. Chem. 10 (2000) 2502.

[13] R. Lv, F. Kang, W. Wang, J. Wei, J. Gu, K. Wang, D. Wu, Carbon 45 (2007) 1433.

[14] X. Gui, K. Wang, W. Wang, J. Wei, X. Zhang, R. Lv, Y. Jia, Q. Shu, F. Kang, D. Wu, Mater. Chem. Phys. 113 (2009) 634.

[15] V. O. Nyamori, S. D. Mhlanga, N. J. Coville, J. Organomet. Chem. 693 (2008) 2205.

[16] E. N. Nxumalo, V. P. Chabalala, V. O. Nyamori, M. J. Witcomb, N. J. Coville, J. Organomet. Chem. 695 (2010) 1451.

[17] E. N. Nxumalo, N. J. Coville, Materials 3 (2010) 2141.

[18] E. N. Nxumalo, V. O. Nyamori, N. J. Coville, J. Organomet. Chem. 693 (2008) 2942.

[19] J. Zhou, J. Lian, L. Hou, J. Zhang, H. Gou, M. Xia, Y. Zhao, T. A. Strobel, L. Tao, F. Gao, Nat. Commun. 6 (2015) 1.

[20] L. M. Ombaka, P. G. Ndungu, B. Omondi, V. O. Nyamori, J. Coord. Chem. 67 (2014) 1905.

[21] S. W. Pattinson, R. E. Diaz, N. A. Stelmashenko, A. H. Windle, C. Ducati, E. A. Stach, K. K. K. Koziol, Chem. Mater. 25 (2013) 2921.

[22] A. Shaikjee, N. J. Coville, Carbon 50 (2012) 3376.

[23] S. W. Pattinson, V. Ranganathan, H. K. Murakami, K. K. K. Koziol, A. H. Windle, ACS Nano 6 (2012) 7723.

[24] L.Chen, K. Xia, L. Huang, L. Li, L. Pei, S. Fei, Int. J. Hydrogen Energy 38 (2013) 3297.

[25] N. Tang, J. Wen, Y. Zhang, F. Liu, K. Lin, Y Du, ACS Nano 4 (2010) 241.

[26] A. Nieto-Màrquez, J. L. Valverde, M. A. Keane, Appl. Catal. A: General 352 (2009) 159.

[27] K. B. Teo, C. Singh, M. Chhowalla, W. I. Milne, Encyclopedia of nanoscience and nanotechnology 10 (2003) 1.

[28] H. T. Chung, P. Zelenay, Chem. Commun. 51 (2015) 13546.

[29] L. Delzeit, I. McAninch, B. A. Cruden, D. Hash, B. Chen, J. Han, M. Meyyappan, J. Appl. Phys. 91 (2002) 6027.

[30] A. C. Ferrari, J. Robertson, Philos. Trans. A Math Phys. Eng. Sci. 362 (2004) 2477.

[31] H. Hiura, T. Ebbesen, K. Tanigaki, H. Takahashi, Chem. Phys. Lett. 202 (1993) 509.

[32] K. A. Wepasnick, B. A. Smith, J. L. Bitter, D. H. Fairbrother, Anal. Bioanal. Chem. 396 (2010) 1003.

[33] Y. Liu, C. Pan, J. Wang, J. Mater. Sci. 39 (2004) 1091.

[34] N. Ramoraswi, P. Ndungu, Nanoscale Res. Lett. 10 (2015) 427.

[35] T. Sharifi, F. Nitze, H. R. Barzegar, C.-W. Tai, M. Mazurkiewicz, A. Malolepszy, L. Stobinski, T. Wågberg, Carbon 50 (2012) 3535.

[36] L. M. Ombaka, P. G. Ndungu, V. O. Nyamori, RSC Adv. 5 (2015) 109.

[37] K. Chizari, A. Vena, L. Laurentius, U. Sundararaj, Carbon 68 (2014) 369.

[38] S. Santangelo, M. Lanza, C. Milone, J. Phys. Chem. C 117 (2013) 4815.

[39] U.-J. Kim, C. A. Furtado, X. Liu, G. Chen, P. C. Eklund, J. Am. Chem. Soc. 127 (2005) 15437.

[40] L. Vanyoreka, R. Meszarosa, S. Barany, Colloids and Surfaces A: Physicochem. Eng. Aspects 448 (2014) 140.

[41] A. Misra, P. K. Tyagi, M. K. Singh, D. S. Misra, Diamond Relat. Mater. 15 (2006) 385.

[42] T. Maiyalagan, B. Viswanathan, Mater. Chem. Phys. 93 (2005) 291.

[43] T. J. Bandosz (2009) Surface chemistry of carbon materials. In: Serp P, Fiueiredo JL (Eds.), Carbon materials fo catalysis. John Wiley & Sons, Inc. United States of America, pp 63.

[44] U. Ritter, N. G. Tsierkezos, Yu. I. Prylutskyy, L. Y. Matzui, V. O. Gubanov, M. M. Bilyi, M. O. Davydenko, J. Mater. Sci. 47 (2012) 2390.

[45] W. Xia, Catal. Sci. Technol. (2016) *In press*. : DOI: 10.1039/c5cy01694k

[46] J. P. ÓByrne, Z. Li, S. L. T. Jones, P. G. Fleming, J. A. Larsson, M. A. Morris, J. D. Holmes, ChemPhysChem 12 (2011) 2995.

[47] W. Xia, X. Yin, S. Kundu, M. Sanchez, A. Birkner, C. Woll, M. Muhler, Carbon 49 (2011) 299.

[48] Z. Luo, S. Lim, Z. Tian, J. Shang, L. Lai, B. MacDonald, C. Fu, Z. Shen, T. Yu, J. Lin, J. Mater. Chem. 21 (2011) 8038.

[49] Y. Yao, B. Zhang, J. Shi, Q. Yang, ACS Appl. Mater Interfaces 7 (2015) 7413.

[50] E. T. Kang, K. G. Neoh, S. H. Khor, K. L. Tan, B. T. G. Tan, Polymer 31 (1990) 202.

[51] Z, Lin, G.H. Waller, Y. Liu, M. Liu, C.-P. Wong, Carbon 53 (2013) 130e6.

[52] Y. Cao, H. Yu, J. Tan, F. Peng, H. Wang, J. Li, W. Zheng, N.-B. Wong, Carbon 57 (2013) 433.

[53] Bruker (2008) APEX2, SAINT-Plus, XPREP and SADABS. Bruker AXS Inc., Madison, Wisconsin, USA.

[54] G. M. Sheldrick, Acta Cryst. A64 (2008) 112.

[55] L. J. Farrugia, J. Appl. Cryst. 32 (1999) 837.

[56] L. J. Farrugia, J. Appl. Cryst. 30 (1997) 565.

[57] R. S. Oosthuizen, V. O. Nyamori, Appl. Organomet. Chem. 26 (2012) 536.

Highlights

1. N-CNTs were synthesized from halogenated ferrocenyl catalysts.
2. Halogenated catalysts promote nitrogen-doping and pyridinic nitrogen in N-CNTs.
3. Halogenated catalysts facilitate iron filling of N-CNTs.

Graphical abstract

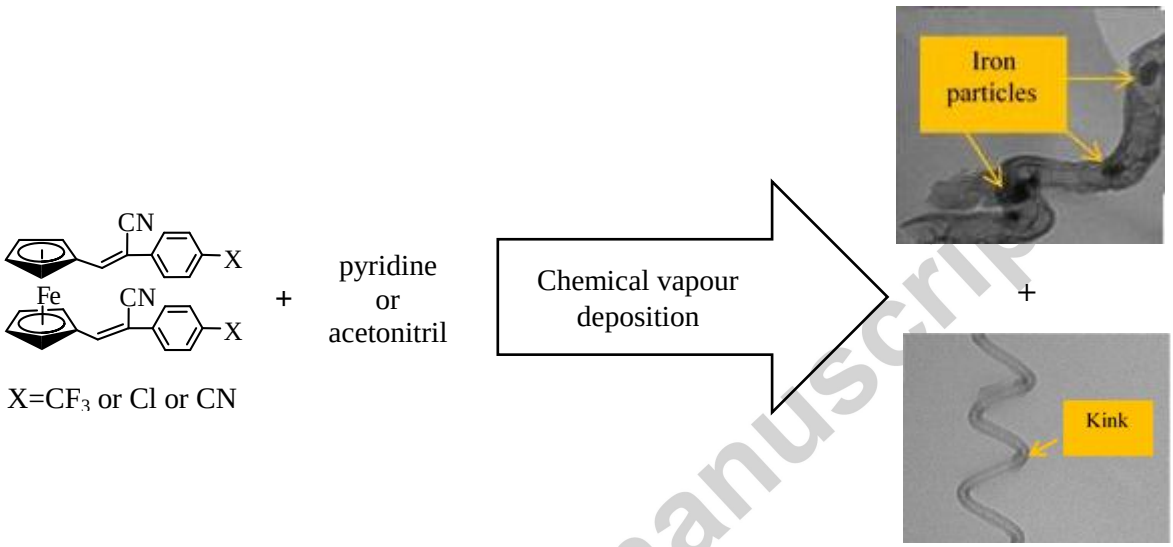

Graphical abstract showing the synthesis of N-CNTs using halogenated-ferrocenyl derivatives as catalyst with pyridine or acetonitrile as nitrogen and carbon sources *via* the chemical vapour deposition technique